

Article

Stagnation Point Flow with Time-Dependent Bionanofluid Past a Sheet: Richardson Extrapolation Technique

Kohilavani Naganthran ¹, Md Faisal Md Basir ², Sayer Obaid Alharbi ³, Roslinda Nazar ¹, Anas M. Alwatban ⁴ and Iskander Tlili ^{5,6,*}

¹ Centre for Modelling and Data Science, Faculty of Science & Technology, Universiti Kebangsaan Malaysia, 43600 UKM Bangi, Selangor, Malaysia; kohi_kk@yahoo.com (K.N.); rmn@ukm.edu.my (R.N.)

² Department of Mathematical Sciences, Faculty of Science, Universiti Teknologi Malaysia, 81310 UTM Johor Bahru, Johor, Malaysia; mfaisalmbasir@utm.my

³ Mathematics Department, College of Science Al-Zulfi, Majmaah University, Majmaah 11952, Saudi Arabia; so.alharbi@mu.edu.sa

⁴ Mechanical Engineering Department, College of Engineering, Qassim University, Qassim 52571, Saudi Arabia; alwatban@qec.edu.sa

⁵ Department for Management of Science and Technology Development, Ton Duc Thang University, Ho Chi Minh City 758307, Vietnam

⁶ Faculty of Applied Sciences, Ton Duc Thang University, Ho Chi Minh City 758307, Vietnam

* Correspondence: iskander.tlili@tdtu.edu.vn

Received: 9 September 2019; Accepted: 30 September 2019; Published: 11 October 2019



Abstract: The study of laminar flow of heat and mass transfer over a moving surface in bionanofluid is of considerable interest because of its importance for industrial and technological processes such as fabrication of bio-nano materials and thermally enhanced media for bio-inspired fuel cells. Hence, the present work deals with the unsteady bionanofluid flow, heat and mass transfer past an impermeable stretching/shrinking sheet. The appropriate similarity solutions transform the boundary layer equations with three independent variables to a system of ordinary differential equations with one independent variable. The finite difference coupled with the Richardson extrapolation technique in the Maple software solves the reduced system, numerically. The rate of heat transfer is found to be higher when the flow is decelerated past a stretching sheet. It is understood that the state of shrinking sheet limits the rate of heat transfer and the density of the motile microorganisms in the stagnation region.

Keywords: bioconvection; boundary layer; nanofluid; stagnation-point flow; stretching/shrinking sheet

1. Highlights

- Validation of the general model has been achieved with the finite-difference coupled with the Richardson extrapolation and the shooting method in the Maple software.
- The far-field boundary conditions were chosen with the appropriate finite value to ensure that the numerical solution ideally approaches the asymptotic values.
- The state of shrinking sheet limits the rate of heat transfer and the density of the motile microorganisms in the stagnation region.

2. Introduction

Nanofluid is a well-known smart fluid which has been found to be very useful in uplifting people's lifestyle. This smart fluid is dilute liquid-suspended nanoparticles, where at least one of their primary measurements is smaller than 10 nm [1]. Nanofluid, as an advanced type of fluids, has been synthesized by dispersing nanoscale particles in conventional base fluids such as water, ethylene glycol, and oil [2]. Recent literature is densely occupied with the investigations of the fluid flow and heat transfer in the nanofluids due to their diverse applications in industry and engineering, compared to investigations about macro-sized materials [3,4]. Nanofluid detergent, nanofluid coolant, nano cryosurgery, and usage of nanofluid for industrial cooling are some of the remarkable applications involving nanofluid [1]. Nanofluid was proposed initially by Choi and Eastman [2] who proved that it has better heat transfer features compared to the conventional base fluids. The work of Buongiorno [5] molded the idea of nanofluid into a mathematical model that focuses on two main slip mechanisms (Brownian diffusion and thermophoresis), later known as the Buongiorno model, which became one of the benchmark models in the theoretical work of the boundary layer flow in a nanofluid. Moreover, the series of paper by Mahian et al. [6,7] provided a critical review on fundamentals, theory and applications of the mathematical modelling and simulations of nanofluid flows, and hence established a strong foundation in the theoretical works on nanofluids [8–13].

The industrial applications such as melt-spinning, wire-drawing, and production of plastic and rubber sheets provoked researchers to investigate the fluid flow and heat transfer past a moving surface. Sakiadis [14,15] formulated the problem of laminar and turbulent boundary layer flow along with a non-stop moving of the flat plate, which can be found in the continuous polymer sheet extrusion from a die. Then, Crane [16] extended the work of Sakiadis [14,15] by setting the sheet velocity to increase proportionally with the distance from a fixed source of flow and presented the closed form of two-dimensional Navier–Stokes equation's analytic solution. Carragher and Crane [17] improved the work of Crane [16] by considering heat transfer property along with a continuous stretching sheet. Those works have been the mainstay for many numerical investigations which undergo various modifications in the scope of the boundary layer (see [18–20]). On the other hand, the fluid flow and heat transfer past a shrinking surface also received much attention from the researchers as they have various significant industrial applications [21–27]. The paper by Muhaimin et al. [28] acknowledged the shrinking surface applications such as shrinking transistors, non-radiated heat-shrinkable polyvinyl chloride (PVC) tubes and shrinking film. The numerical study of Davey [29] on the boundary layer flow past a shrinking surface which revealed the presence of dual solutions had initiated the development of the fluid flow and heat transfer past a shrinking surface. Goldstein [30] also focused on the backward boundary layer flow in a narrowing channel and discovered that the shrinking fluid flow postulates different physical behavior than the fluid flow caused by the stretching sheet.

Envision the behavior of the microorganisms which are slightly denser than water swimming upward. When more microorganisms accumulate at the upper region, that area becomes denser until at one point the suspensions turn out to be unbalanced. Consequently, the microorganisms tumble and form a bioconvection. In the experimental approach, two usual types of upswimming microorganisms: bottom-heavy alga (*Chlamydomonas nivalis*) and common soil bacterium *Bacillus subtilis*, are considered [31]. Different types of microorganisms own the subjective orientation of the mechanism [32]. For the theoretical study, the conventional mathematical model instituted bottom-heavy alga and oxytactic bacteria. The development of theoretical work in the field of bioconvection can be found in the following literature: [33–45]. Kuznetsov [46] commenced the problem of bioconvection boundary layer flow along a horizontal surface in a nanofluid containing a gyrotactic microorganism and presented the perturbation solutions. After that, Zaimi et al. [47] extended the work of Kuznetsov [46] by considering a stagnation-point bioconvection flow past a permeable stretching/shrinking surface in a nanofluid. Zaimi et al. [47] which had solved the problem numerically by using the shooting method in the Maple software and had presented dual solutions concluded that the influence of suction is essential to maintain a laminar boundary layer

flow. The present paper aimed to broaden the research work of Zaimi et al. [47] by examining an unsteady stagnation-point flow past an impermeable stretching/shrinking sheet in a nanofluid containing gyrotactic microorganisms. The numerical solutions are produced via the Richardson extrapolation technique, and the effects of variations of the governing parameters on the physical quantities have been presented graphically and discussed in detail.

3. Mathematical Formulation

The present theoretical model considers an unsteady two-dimensional boundary layer flow and heat transfer at the stagnation region induced by a moving (stretching/shrinking) surface in a water-based nanofluid. Bionanofluid comprises of nanoparticles and motile gyrotactic microorganisms and allows the bioconvection process. In this investigation, water was chosen as the working fluid to keep the gyrotactic microorganisms alive, while the presence of the nanoparticles does not affect the gravitactic microorganisms' swimming route and velocity. The nanosized (1–100 nm) metal nanoparticles which are made from metal precursors such as copper are considered in this investigation. Theoretically, the concentration of the nanoparticles is assumed to be $\leq 1\%$ [5]. The physical configuration of the problem is shown in Figure 1.

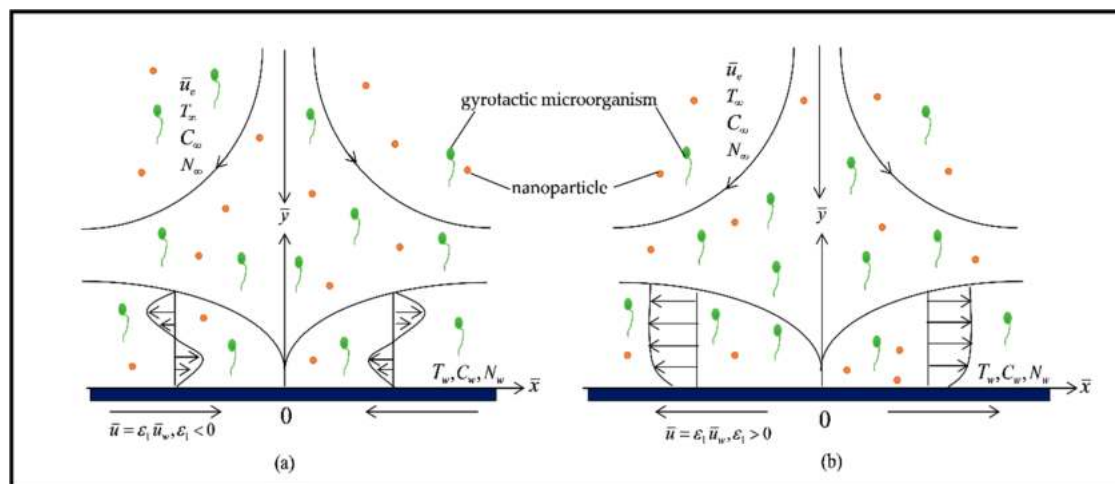


Figure 1. Schematic diagram of the problem. (a) Shrinking case. (b) Stretching case.

The Cartesian coordinate frame is taken, where the \bar{x} - direction remains along the stretching/shrinking surface, and the \bar{y} - direction stands perpendicular to the surface. It is presumed that the sheet is stretching/shrinking with a velocity $\bar{u}_w = \varepsilon_1 a \bar{x} (1 - A_1 \bar{t})^{-1}$, in which a is a positive constant with dimension (s^{-1}), $\varepsilon_1 > 0$ shows the stretching sheet, $\varepsilon_1 < 0$ indicates the shrinking sheet while $\varepsilon_1 = 0$ represents a stationary sheet. The ambient velocity is given as $\bar{u}_w = a \bar{x} (1 - A_1 \bar{t})^{-1}$. In addition, the temperature, nanoparticle concentration and the density of microorganisms far away from the surface of the sheet are denoted as T_∞, C_∞ and N_∞ , respectively. The temperature, nanoparticle concentration and the density of microorganisms at the wall of the moving surface are symbolized as T_w, C_w and N_w , respectively. It is assumed that $T_w > T_\infty, C_w > C_\infty, N_w > N_\infty$ and boundary conditions are applied to the surface of the sheet, with no-slip conditions. The thin moving sheet acts to heat the infinite body of fluid and retains a constant temperature throughout the process. The heating is adequately weak thus preserving the living gyrotactic microorganisms within the stagnation area. Based on these assumptions, the governing boundary layer equations can be given as follows [47]:

$$\frac{\partial \bar{u}}{\partial \bar{x}} + \frac{\partial \bar{v}}{\partial \bar{y}} = 0, \quad (1)$$

$$\frac{\partial \bar{u}}{\partial \bar{t}} + \bar{u} \frac{\partial \bar{u}}{\partial \bar{x}} + \bar{v} \frac{\partial \bar{u}}{\partial \bar{y}} = \bar{u}_e \frac{\partial \bar{u}_e}{\partial \bar{x}} + \frac{\partial \bar{u}_e}{\partial \bar{t}} + v \left(\frac{\partial^2 \bar{u}}{\partial \bar{y}^2} \right), \quad (2)$$

$$\frac{\partial T}{\partial \bar{t}} + \bar{u} \frac{\partial T}{\partial \bar{x}} + \bar{v} \frac{\partial T}{\partial \bar{y}} = \alpha \frac{\partial^2 T}{\partial \bar{y}^2} + \tau_1 \left[D_B \left(\frac{\partial T}{\partial \bar{y}} \frac{\partial C}{\partial \bar{y}} \right) + \frac{D_T}{T_\infty} \left(\frac{\partial T}{\partial \bar{y}} \right)^2 \right], \quad (3)$$

$$\frac{\partial C}{\partial \bar{t}} + \bar{u} \frac{\partial C}{\partial \bar{x}} + \bar{v} \frac{\partial C}{\partial \bar{y}} = D_B \left(\frac{\partial^2 C}{\partial \bar{y}^2} \right) + \frac{D_T}{T_\infty} \left(\frac{\partial^2 T}{\partial \bar{y}^2} \right), \quad (4)$$

$$\frac{\partial N}{\partial \bar{t}} + \bar{u} \frac{\partial N}{\partial \bar{x}} + \bar{v} \frac{\partial N}{\partial \bar{y}} + \frac{\tilde{b} W_c}{C_w - C_\infty} \left[\frac{\partial}{\partial \bar{y}} \left(N \frac{\partial C}{\partial \bar{y}} \right) \right] = D_n \left(\frac{\partial^2 N}{\partial \bar{y}^2} \right). \quad (5)$$

Hence, the relevant boundary conditions are represented by

$$\begin{aligned} t \leq 0: \quad & \bar{v} = 0, \bar{u} = 0, T = T_\infty, C = C_\infty, N = N_\infty. \\ t > 0: \quad & \bar{u} = \varepsilon_1 \bar{u}_w(x, t) = \varepsilon_1 a \bar{x} (1 - A_1 \bar{t})^{-1} \text{ with } A_1 \bar{t} \neq 1, \bar{v} = 0, T = T_w, \\ & C = C_w, N = N_w \quad \text{at } \bar{y} = 0, \\ & \bar{u} = \bar{u}_e(x, t) = a \bar{x} (1 - A_1 \bar{t})^{-1} \text{ with } A_1 \bar{t} \neq 1, T = T_\infty, \\ & C = C_\infty, N = N_\infty \quad \text{as } \bar{y} \rightarrow \infty, \end{aligned} \quad (6)$$

where \bar{u} and \bar{v} are the velocity components along the \bar{x} - and \bar{y} - axes, respectively, \bar{t} is time, v is the kinematic viscosity, T is the temperature, α is the thermal diffusivity of the nanofluid, C is the nanoparticle volume fraction, $\tau_1 = (\rho c)_p / (\rho c)_f$ is the ratio between the heat capacity of the nanoparticle $(\rho c)_p$ and the heat capacity of the base fluid $(\rho c)_f$, D_B is the Brownian diffusion coefficient, D_T is the thermophoretic diffusion coefficient, N is the number density of motile microorganisms, D_n is the diffusivity of microorganism, \tilde{b} is the chemotaxis constant, W_c is the maximum cell swimming speed relative to the nanofluid and A_1 is a constant with dimension $(\text{time})^{-1}$ which denotes the unsteadiness of the problem.

4. Similarity Differential Equations

Revised from Ali and Zaib [48], we adopt the following similarity transformations:

$$\begin{aligned} \eta &= \left(\frac{a}{v(1-A_1 \bar{t})} \right)^{1/2} \bar{y}, \quad \psi = \left(\frac{av}{1-A_1 \bar{t}} \right)^{1/2} \bar{x} f(\eta), \\ \theta(\eta) &= \frac{T-T_\infty}{T_w-T_\infty}, \quad \phi(\eta) = \frac{C-C_\infty}{C_w-C_\infty}, \quad \chi(\eta) = \frac{N}{N_w}. \end{aligned} \quad (7)$$

The substitution of the similarity solution (7) into the system (1)–(6), satisfies Equation (1) and the rest of the expressions are transformed as follows:

$$f''' + f f'' - f'^2 + 1 + A \left[1 - \left(\frac{1}{2} \eta f'' + f' \right) \right] = 0, \quad (8)$$

$$\theta'' + \text{Pr} f \theta' + \text{Nb} \theta' \phi' + \text{Nt} \theta'^2 - \frac{1}{2} \text{Pr} A \eta \theta' = 0, \quad (9)$$

$$\phi'' + \frac{\text{Nt}}{\text{Nb}} \theta'' + \text{Le} \text{Pr} f \phi' - \frac{1}{2} \text{Le} \text{Pr} A \eta \phi' = 0, \quad (10)$$

$$\chi'' + \text{Lb} \text{Pr} f \chi' - \text{Pe} [\chi \phi'' + \phi' \chi'] - \frac{1}{2} \text{Lb} \text{Pr} \eta A \chi' = 0, \quad (11)$$

along with the boundary conditions

$$\begin{aligned} f(0) &= 0, f'(0) = \varepsilon_1, \theta(0) = 1, \phi(0) = 1, \chi(0) = 1, \\ f'(\infty) &= 1, \theta(\infty) = \phi(\infty) = \chi(\infty) = 0, \end{aligned} \quad (12)$$

where the Prandtl number (Pr), the Brownian motion parameter (Nb), the thermophoresis parameter (Nt), the Lewis number (Le), the bioconvection Lewis number (Lb) and the Péclet number (Pe) are defined as

$$\begin{aligned} Pr &= \frac{\nu}{\alpha}, \quad Nb = \frac{\tau D_B (C_w - C_\infty)}{\alpha}, \quad Nt = \frac{\tau D_T (T_w - T_\infty)}{\alpha T_\infty}, \\ Le &= \frac{\alpha}{D_B}, \quad Lb = \frac{\alpha}{D_n}, \quad Pe = \frac{\tilde{b} W_c}{D_n}. \end{aligned} \quad (13)$$

Meanwhile, $A > 0$ corresponds to an accelerated flow and $A < 0$ connotes a decelerated flow. For $A = 0$, the flow is steady, i.e., the flow is independent of time.

5. Physical Quantities

The physical quantities of engineering interest in this study are the local skin friction coefficient ($C_{f_{\bar{x}}}$), the local Nusselt number ($Nu_{\bar{x}}$), the local Sherwood number ($Sh_{\bar{x}}$), and the local density number of motile microorganisms ($Nn_{\bar{x}}$), defined as [47]

$$C_{f_{\bar{x}}} = \frac{\mu \frac{\partial \bar{u}}{\partial \bar{y}} \Big|_{\bar{y}=0}}{\rho \bar{u}_e^2}, \quad Nu_{\bar{x}} = \frac{\bar{x} \left(-k \frac{\partial T}{\partial \bar{y}} \Big|_{\bar{y}=0} \right)}{k(T_w - T_\infty)}, \quad Sh_{\bar{x}} = \frac{\bar{x} \left(-D_B \frac{\partial C}{\partial \bar{y}} \Big|_{\bar{y}=0} \right)}{D_B(T_w - T_\infty)}, \quad Nn_{\bar{x}} = \frac{\bar{x} \left(-D_n \frac{\partial N}{\partial \bar{y}} \Big|_{\bar{y}=0} \right)}{D_n(N_w)}. \quad (14)$$

The substitution of Equation (7) into (14) yield the following expressions:

$$Re_{\bar{x}}^{1/2} C_{f_{\bar{x}}} = f''(0), \quad Re_{\bar{x}}^{-1/2} Nu_{\bar{x}} = -\theta'(0), \quad Re_{\bar{x}}^{-1/2} Sh_{\bar{x}} = -\phi'(0), \quad Re_{\bar{x}}^{-1/2} Nn_{\bar{x}} = -\chi'(0), \quad (15)$$

where the local Reynolds number is given as $Re_{\bar{x}} = \frac{\bar{u}_e \bar{x}}{\nu}$.

6. Computational Method and Validation

The boundary value problem (8)–(12) was solved numerically by using a finite-difference technique, namely the Richardson extrapolation in the Maple software. This technique is a sequence acceleration method which is used to improve the rate of convergence of a sequence. The Richardson extrapolation (also known as post-processing procedure) is capable of producing a better accuracy to the exact solution obtained by averaging the computed numerical results on two embedded meshes [49]. The built-in command in Maple, dsolve uses the Richardson extrapolation technique to solve the boundary value problem efficiently. Based on the results of previous studies published by Zaimi et al. [47] and Ibrahim et al. [50], a comparison is made for the values of $f''(0)$, $-\theta'(0)$ and $-\phi'(0)$, as shown in Table 1. There is an excellent agreement with the numerical values reported by previous literature which employed the shooting method. Numerically, the non-linear differential equation system (8)–(11) was solved by the conditions of associated boundary (12) by utilizing the finite-difference technique coupled with Richardson extrapolation numerical method. In this study, the specific range of the boundary layer thickness, η_∞ , was used in the computation and depends on the values of the parameters considered to ensure that all numerical solutions approach the asymptotic values correctly.

Table 1. Comparison of $f''(0)$, $-\theta'(0)$ and $-\phi'(0)$ when $\varepsilon_1 = 1$, $Pe = 1$, $Le = 2$, $Sc = 1$, $A = 0$, $Nt = Nb = 0.5$, and $Pr = 1$ in Equations (8)–(12) and setting $M = 0$ and $A = 1$ in Equations (18) and (21) of the paper by Ibrahim et al. [50].

	Ibrahim et al. [50]	Zaimi et al. [47]	Present Results
$f''(0)$	0	0	0
$-\theta'(0)$	0.4767	0.476737	0.476737
$-\phi'(0)$	1.0452	1.045154	1.045154

7. Results and Discussion

The computation process was carried out by setting $Pr = 6.8$ and $A = 0.5$ to signify water-based nanofluid and decelerated flow, respectively. Figure 2a–c presents the temperature, concentration, and the density of motile microorganisms profiles as the Brownian motion parameter (Nb) varies for the case of stretching sheet ($\varepsilon_1 = 0.5$) and shrinking sheet ($\varepsilon_1 = -0.5$). The temperature profiles as in Figure 2a convey that an increment in Nb at a stretching and shrinking sheet increases the bionanofluid temperature. The stretching sheet results in a thinner thermal boundary layer and steeper profiles compared to the profiles of the shrinking sheet. The state of shrinking sheet, which increases the fluid temperature, causes the temperature gradient to decline and reduces the rate of convective heat transfer. Figure 2b reveals that the decrement of the nanoparticle concentration as the values of Nb increase past a stretching and shrinking sheet. The increment in Nb creates continuous collisions between the nanoparticles and the water molecules, which induce the molecules to move more aggressively. Consequently, the nanoparticles, which had gained kinetic energy, move away from the surface of the moving sheet and result in the depletion of the concentration profiles as Nb increases. Physically larger values of Nb correlate with the nanoparticles of smaller sizes. This phenomenon promotes thermal conduction and macro-convection that has been explained in detail by Buongiorno [5], and also promotes nanoparticle species' diffusion in nanofluid's main body, i.e., more remote from a wall. Figure 2c illustrates the decrement of the density of motile microorganisms as the values of Nb increases. This trend is same for both cases of stretching and shrinking sheets. It is apparent from Figure 2c that the density of microorganisms at a surface sheet maximizes ($\chi = 1$) for the shrinking sheet; on the other hand, the density of microorganisms at a sheet surface is minimized as Nb is enhanced. From the results, it can be concluded that microorganisms have a propensity to swim further away from a sheet surface, especially in a condition where the sheet is shrinking in the boundary layer. Hence, this leads to making microorganisms' density at the wall lower in contrast to the case of a stretching sheet. High Nb values enhance the thickness of the nanoparticle concentration boundary layer as they are dominant influencers; conversely, nanoparticle concentration (shrinking sheet) in the boundary layer is decreased by higher Nb values.

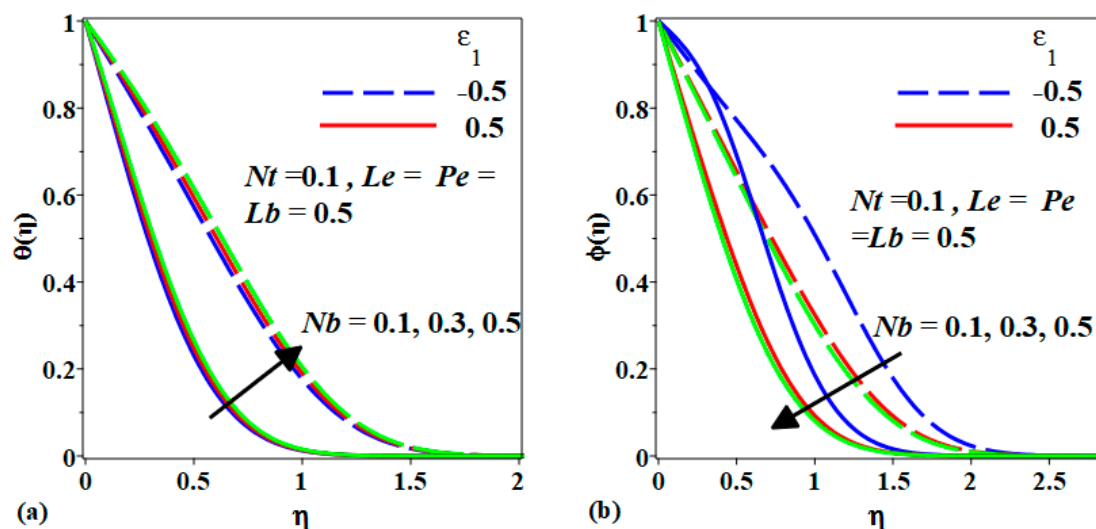


Figure 2. Cont.

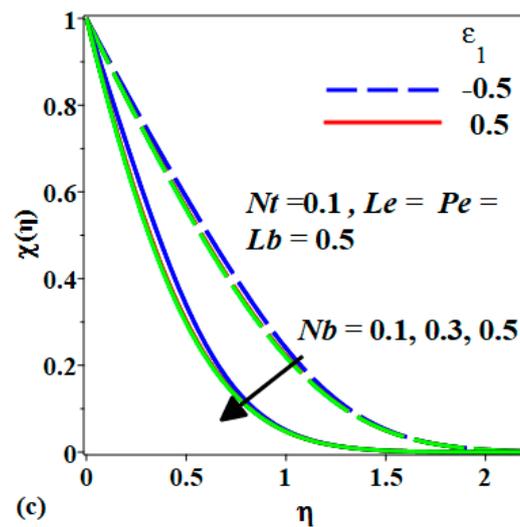


Figure 2. Variation of Nb and ε_1 on (a) $\theta(\eta)$; (b) $\phi(\eta)$; (c) $\chi(\eta)$.

The effects of the thermophoresis (Nt) parameter towards the temperature, concentration, and the density of motile microorganisms' profiles are plotted in Figure 3a–c, respectively for the stretching and shrinking sheet cases. Based on Figure 3a–c, increments are noted in temperature, concentration and microorganism density when the value of the thermophoresis parameter increases. The increment of Nt indicates a stronger thermophoretic force (due to the temperature gradient) which displaces the nanoparticles away from the hot sheet to quiescent fluid, which increases the concentration of the nanoparticles. The augmentation of the nanoparticles' volume fraction greater than unit presented in Figure 3b is not acceptable because theoretically, the concentration of the nanoparticles should be ≤ 1 where $\phi = 1$ expresses that there is no fluid and the material entirely consists of solid particles. The concentration profiles for the shrinking case, as shown in Figure 3b, portray values of the nanoparticles' concentration greater than one, and this is due to the concentration overshoot along the shrinking surface which forms the backward flow that later may disrupt the laminar flow.

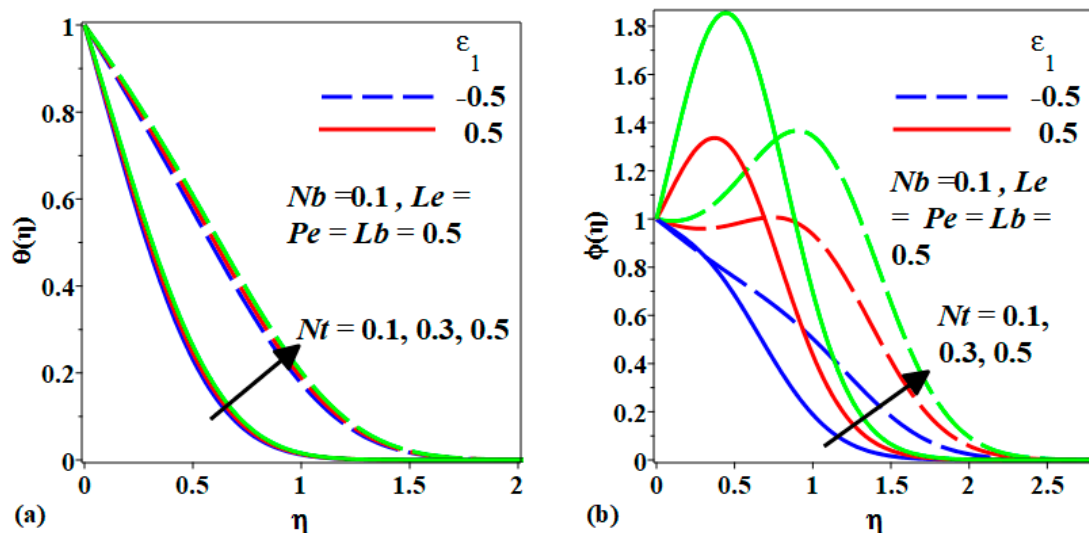


Figure 3. Cont.

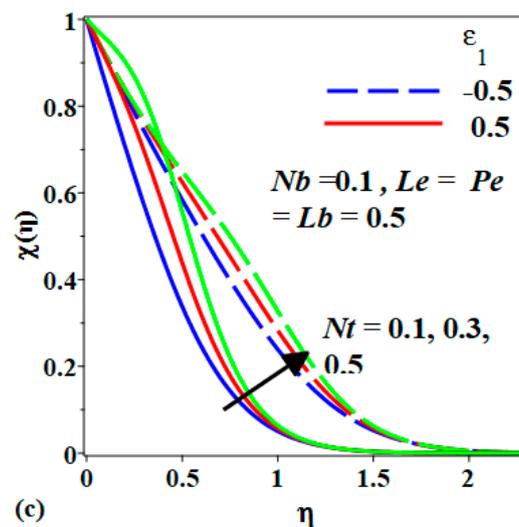


Figure 3. Variation of Nt and ε_1 on (a) $\theta(\eta)$; (b) $\phi(\eta)$ and (c) $\chi(\eta)$.

Figure 4 suggests the depreciation of the concentration by the increment of the Lewis number (Le). The thickness of the concentration boundary layer decreases with an increment of Lewis number. The Lewis number encodes the thermal diffusion's relative strength to the nanoparticle diffusion rates. If a condition happened to be $Le > 1$, the thermal diffusivity would exceed the nanoparticle diffusivity. As a result, this leads to improvement in nanoparticles' magnitudes in the stagnation regime, as well as accentuation in the concentration boundary layer thickness.

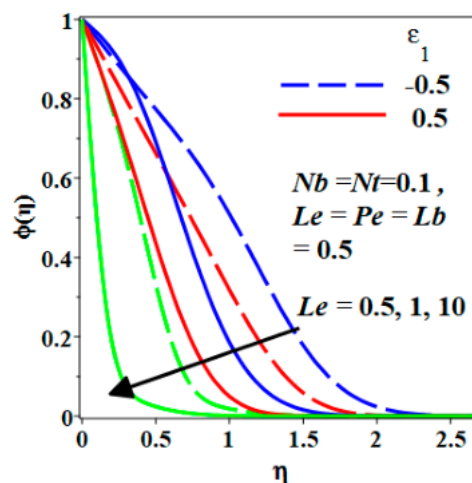


Figure 4. Variation of Le and ε_1 on $\phi(\eta)$.

Figures 5 and 6 show the distributions of the motile microorganism rescaled density function, $\chi(\eta)$ with diverse bioconvection Lewis (Lb) and Péclet (Pe) numbers for both cases of stretching and shrinking cases. Figures 5 and 6 exhibit that an increment of Pe and Lb decreases the density of motile microorganisms. In parallel with this circumstance, the motile microorganism rescaled density function is usually enhanced by mounting bioconvection Lewis numbers. Pe connects a flow's advection rate to its diffusion rate. Since $Pe = \tilde{b}W_c/D_n$, particularly when the chemotaxis is constant, it is directly proportional to the steady maximum cell swimming speed and inversely proportional to D_n (microorganisms' diffusivity). As $Pe > 1$, swimming movements have control over microorganisms' species diffusivity. These eventually promote a decrease in the density of motile microorganism. Increasing bioconvection Lewis number's (Lb) effects of aiding are held responsible for the decrement in microorganisms' diffusivity relative to microorganism's effective thermal diffusivity. Increasing

bioconvection Lewis and Péclet (Pe) numbers suppressed a motile microorganism rescaled density boundary layer thickness.

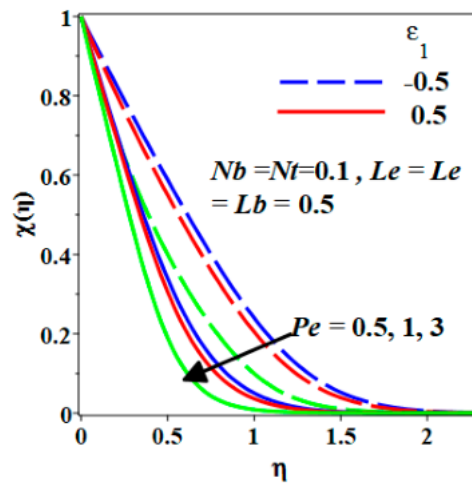


Figure 5. Variation of Pe and ε_1 on $\chi(\eta)$.

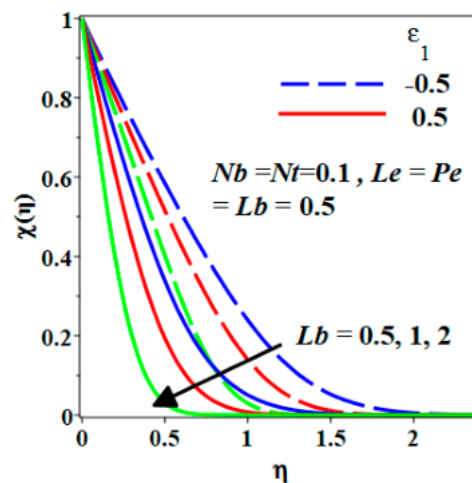


Figure 6. Variation of Lb and ε_1 on $\chi(\eta)$.

The temperature gradient is observed to be enhanced with negative A (decelerated flow) and reduced when $A = 0$ (steady). The state of the stretching surface, however, results in a rise in temperature gradient for both negative and zero values of A , whereas the shrinking sheet wall results in a substantial drop in the temperature gradient (Figure 7). In Figure 8, the mass transfer rate response to variation of the unsteadiness parameter (A), Lewis number (Le) and wall stretching/shrinking (ε_1) effects is shown. With the negative values of ε_1 (shrinking effect), the mass transfer rate is enhanced, whereas the opposite effect is sustained for positive values of ε_1 (stretching effect) in the decelerating case. Microorganism gradient is enhanced in the case of the stretching sheet while it declines with the shrinking surface (Figure 9). For the Maple solutions, the effect of the unsteadiness parameter (A) and the stretching/shrinking parameter (ε_1) on the dimensionless velocity and velocity gradient are not significant.

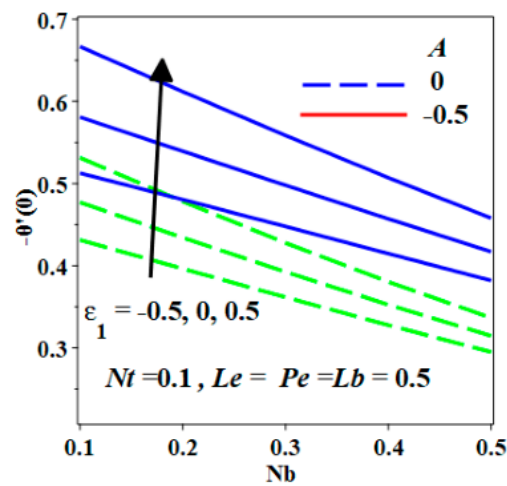


Figure 7. Variation of A, Nb and ϵ_1 on $-\theta'(0)$.

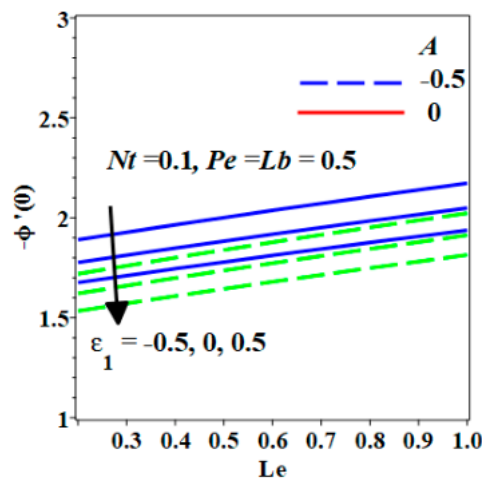


Figure 8. Variation of A, Le and ϵ_1 on $-\phi'(0)$.

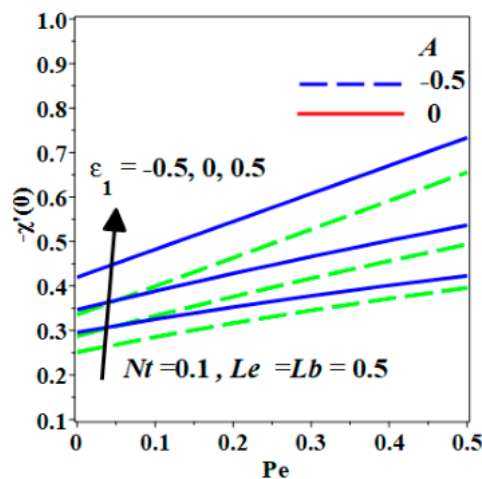


Figure 9. Variation of A, Pe and ϵ_1 on $-\chi'(0)$.

8. Conclusions

This present work attempts to solve the problem of the unsteady stagnation-point and heat transfer past a stretching/shrinking sheet in a nanofluid containing gyrotactic microorganisms. The finite-difference method, namely the Richardson extrapolation technique in the Maple software,

has been employed to solve the model in the form of ordinary differential equations. The numerical results were organized in terms of profiles and the physical quantities' characteristics. This theoretical work is relevant to improve the performance of micro-scale mixing device, based on stable water suspensions of nanoparticles and microorganisms. The outcomes of the present investigation are summarized as follows:

- The increment in Nb past a stretching or shrinking sheet increases the temperature of the bionanofluid temperature but decreases the nanoparticle concentration and the density of motile microorganisms,
- The enhancement in Nt improves the fluid temperature, concentration and the microorganism density in the stagnation region.
- The increment of Le affects the concentration of the nanoparticles, causing it to decrease.
- The increment of Pe and Lb decreases the density of motile microorganisms past a stretching or shrinking sheet.
- The microorganism diffusivity is high in the case the stretching sheet but low in the case of the shrinking sheet.

Author Contributions: K.N.; R.N.; M.F.M.B.; A.M.A.; S.O.A. and I.T. modeled the problem, numerically computed results, discussed the results physically, computed the tabulated results, wrote the manuscript and proof read it.

Funding: This research was funded by Universiti Kebangsaan Malaysia, grant number [DIP-2017-009].

Acknowledgments: The authors are thankful to the honorable reviewers for their constructive suggestions to improve the quality of the paper. The authors from the Universiti Kebangsaan Malaysia would like to acknowledge the research university grant from the Universiti Kebangsaan Malaysia (project code: DIP-2017-009).

Conflicts of Interest: The authors declare no conflict of interest.

Nomenclature

a	Dimensional positive constant (s^{-1})
A	Unsteadiness parameter
A_1	Dimensional constant (s^{-1})
\tilde{b}	Chemotaxis constant (m)
C	Nanoparticles concentration
$C_{f\bar{x}}$	Skin friction coefficient
C_w	Nanoparticle concentration at the stretching/shrinking surface
C_∞	Ambient nanoparticle concentration
D_B	Brownian diffusion coefficient (m^2s^{-1})
D_m	Diffusivity of microorganism (m^2s^{-1})
D_n	Diffusivity coefficient (m^2s^{-1})
D_T	Thermophoresis diffusion coefficient (m^2s^{-1})
k	Thermal conductivity ($Wm^{-1}K^{-1}$)
Lb	bioconvection Lewis number
N	Concentration of the microorganisms
$Nn_{\bar{x}}$	Local density number of the motile microorganism
N_w	Microorganisms at the sheet
N_∞	Microorganisms far from the sheet
Nb	Brownian motion parameter
$Nu_{\bar{x}}$	Local Nusselt number
Nt	Thermophoresis parameter
Pe	Dimensionless Péclet number
Pr	Prandtl number
$Re_{\bar{x}}$	Local Reynolds number
$Sh_{\bar{x}}$	Local Sherwood number
T	Temperature (K)

\bar{t}	Dimensional time (s)
T_w	Surface temperature (K)
T_∞	Ambient temperature (K)
\bar{u}_w	Velocity of the sheet (ms^{-1})
W_c	Maximum cell swimming speed (ms^{-1})
(\bar{x}, \bar{y})	Cartesian coordinates (m)
(\bar{u}, \bar{v})	Velocity of the components (ms^{-1})

Greek Letters

α	Thermal diffusivity (m^2s^{-1})
η	Similarity variable (m^2s^{-1})
μ	Dynamic viscosity (Pa s^{-1})
ν	Kinematic viscosity (m^2s^{-1})
ρ	Density (Kgm^{-3})
$(\rho c)_p$	Nanoparticles heat capacity (JK^{-1}m^3)
$(\rho c)_f$	Base fluid heat capacity (JK^{-1}m^3)
ε_1	Stretching/Shrinking parameter
τ_1	Ratio of the effective heat capacitance of the nanoparticle to that of the base fluid
θ	Dimensionless temperature
ϕ	Dimensionless nanoparticle concentration
χ	Dimensionless microorganisms
ψ	Dimensionless stream function

Subscripts

w	condition at the surface
∞, e	condition outside of boundary layer

Superscript

$'$	differentiation with respect to η
-----	--

References

- Wong, K.V.; Leon, O.D. Applications of nanofluids: Current and future. *Adv. Mech. Eng.* **2010**, *2018*, 1–11. [[CrossRef](#)]
- Choi, S.U.S.; Eastman, J.A. Enhancing thermal conductivity of fluids with nanoparticles. *ASME Publ. Fed.* **1995**, *231*, 99–106.
- Molina, J.; Rodríguez-Guerrero, A.; Louis, E.; Rodríguez-Reinoso, F.; Narciso, J. Porosity effect on thermal properties of Al-12 wt% Si/Graphite composites. *Materials* **2017**, *10*, 177. [[CrossRef](#)] [[PubMed](#)]
- Caccia, M.; Camarano, A.; Sergi, D.; Ortona, A.; Narciso, J. Wetting and Navier-Stokes equation—The manufacture of composite materials. *Wetting Wettability* **2015**, 105–137.
- Buongiorno, J. Convective transport in nanofluids. *J. Heat Trans-T ASME* **2006**, *128*, 240–250. [[CrossRef](#)]
- Mahian, O.; Kolsi, L.; Amani, M.; Estellé, P.; Ahmadi, G.; Kleinstreuer, C.; Marshall, J.S.; Siavashi, M.; Taylor, R.A.; Niazmand, H.; et al. Recent advances in modeling and simulation of nanofluid flows-Part I: Fundamentals and theory. *Phys. Rep.* **2019**, *790*, 1–48. [[CrossRef](#)]
- Mahian, O.; Kolsi, L.; Amani, M.; Estellé, P.; Ahmadi, G.; Kleinstreuer, C.; Marshall, J.S.; Taylor, R.A.; Abu-Nada, E.; Rashidi, S.; et al. Recent advances in modelling and simulation of nanofluid flows-Part II: Applications. *Phys. Rep.* **2019**, *791*, 1–59. [[CrossRef](#)]
- Tlili, I. Effects MHD and Heat Generation on Mixed Convection Flow of Jeffrey Fluid in Microgravity Environment over an Inclined Stretching Sheet. *Symmetry* **2019**, *11*, 438. [[CrossRef](#)]
- Goodarzi, M.; Tlili, I.; Tian, Z.; Safaei, M.R. Efficiency assessment of using graphene nanoplatelets-silver/water nanofluids in microchannel heat sinks with different cross-sections for electronics cooling. *Int. J. Numer. Methods Heat Fluid Flow* **2019**. submitted for publication. [[CrossRef](#)]
- Afridi, M.I.; Tlili, I.; Goodarzi, M.; Osman, M.; Alam Khan, N. Irreversibility Analysis of Hybrid Nanofluid Flow over a Thin Needle with Effects of Energy Dissipation. *Symmetry* **2019**, *11*, 663. [[CrossRef](#)]
- Tlili, I.; Alkanhal, T.A. Nanotechnology for water purification: Electrospun nanofibrous membrane in water and wastewater treatment. *J. Water Reuse Desalin.* **2019**, *9*, 232–248. [[CrossRef](#)]

12. Tlili, I.; Khan, W.A.; Ramadan, K. MHD Flow of Nanofluid Flow Across Horizontal Circular Cylinder: Steady Forced Convection. *J. Nanofluids* **2019**, *8*, 179–186. [[CrossRef](#)]
13. Tlili, I.; Khan, W.A.; Ramadan, K. Entropy Generation Due to MHD Stagnation Point Flow of a Nanofluid on a Stretching Surface in the Presence of Radiation. *J. Nanofluids* **2018**, *7*, 879–890. [[CrossRef](#)]
14. Sakiadis, B.C. Boundary-layer behavior on continuous solid surfaces: I. Boundary-layer equations for two-dimensional and axisymmetric flow. *AICHE J.* **1961**, *7*, 26–28. [[CrossRef](#)]
15. Sakiadis, B.C. Boundary-layer behavior on continuous solid surfaces: II. The boundary layer on a continuous flat surface. *AICHE J.* **1961**, *7*, 221–225. [[CrossRef](#)]
16. Crane, L.J. Flow past a stretching plate. *Z. Angew. Math. Phys.* **1970**, *21*, 645–647. [[CrossRef](#)]
17. Carragher, P.; Crane, L.J. Heat transfer on a continuous stretching sheet. *Z. Angew. Math. Phys.* **1982**, *62*, 564–565. [[CrossRef](#)]
18. Pop, I.; Naganthran, K.; Nazar, R. Numerical solutions of non-alignment stagnation point flow and heat transfer over a stretching/shrinking surface in a nanofluid. *Int. J. Numer. Method Heat* **2016**, *26*, 1747–1767. [[CrossRef](#)]
19. Pop, I.; Naganthran, K.; Nazar, R.; Ishak, A. The effect of vertical throughflow on the boundary layer flow of a nanofluid past a stretching/shrinking sheet: A revised model. *Int. J. Numer. Method Heat* **2017**, *27*, 1910–1927. [[CrossRef](#)]
20. Jusoh, R.; Nazar, R.; Pop, I. Flow and heat transfer of magnetohydrodynamic three-dimensional Maxwell nanofluid over a permeable stretching/shrinking surface with convective boundary conditions. *Int. J. Mech. Sci.* **2017**, *124*, 166–173. [[CrossRef](#)]
21. Tlili, I.; Khan, W.A.; Khan, I. Multiple slips effects on MHD SA-Al₂O₃ and SA-Cu non-Newtonian nanofluids flow over a stretching cylinder in porous medium with radiation and chemical reaction. *Results Phys.* **2018**, *8*, 213–222. [[CrossRef](#)]
22. Tlili, I.; Hamadneh, N.N.; Khan, W.A. Khan. Thermodynamic Analysis of MHD Heat and Mass Transfer of Nanofluids Past a Static Wedge with Navier Slip and Convective Boundary Conditions. *Arab. J. Sci. Eng.* **2018**, *4*, 1–13. [[CrossRef](#)]
23. Tlili, I.; Hamadneh, N.N.; Khan, W.A.; Atawneh, S. Thermodynamic analysis of MHD Couette–Poiseuille flow of water-based nanofluids in a rotating channel with radiation and Hall effects. *J. Ther. Anal. Calorim.* **2018**, *132*, 1899–1912. [[CrossRef](#)]
24. Waqar, A.; Khan, A.M.; Rashad, M.M.M.; Abdou, I.T. Natural bioconvection flow of a nanofluid containing gyrotactic microorganisms about a truncated cone. *Eur. J. Mech. -B/Fluids* **2019**, *75*, 133–142. [[CrossRef](#)]
25. Khalid, A.; Khan, A.; Shafie, S.; Tlili, I.; Khan, I. Case study of MHD blood flow in a porous medium with CNTs and thermal analysis. *Case Stud. Therm. Eng* **2018**, *12*, 374–380. [[CrossRef](#)]
26. Bidin, B.; Nazar, R. Numerical solution of the boundary layer flow over an exponentially stretching sheet with thermal radiation. *Eur. J. Sci. Res.* **2009**, *33*, 710–717.
27. Ghasemian, A.; Dinarvand, S.; Adamian, A.; Sheremet, M.A. Unsteady General Three-Dimensional Stagnation Point Flow of a Maxwell/Buongiorno Non-Newtonian Nanofluid. *J. Nanofluids* **2019**, *8*, 1544–1559. [[CrossRef](#)]
28. Kandasamy, R.; Hashim, I. Effect of chemical reaction, heat and mass transfer on nonlinear boundary layer past a porous shrinking sheet in the presence of suction. *Nucl. Eng. Des.* **2010**, *240*, 933–939.
29. Davey, A. Boundary-layer flow at a saddle point of attachment. *J. Fluid Mech.* **1961**, *10*, 593–610. [[CrossRef](#)]
30. Goldstein, S. On backward boundary layers and flow in converging passages. *J. Fluid Mech.* **1965**, *21*, 33–45. [[CrossRef](#)]
31. Hill, N.A.; Pedley, T.J. Bioconvection. *Fluid. Dyn. Res.* **2005**, *37*, 1–20. [[CrossRef](#)]
32. Pedley, T.J.; Kessler, J.O. The orientation of spheroidal microorganisms swimming in a flow field. *Proc. R. Soc. Lond.* **1987**, *231*, 47–70.
33. Pedley, T.J.; Hill, N.A.; Kessler, J.O. The growth of bioconvection patterns in a uniform suspension of gyrotactic microorganisms. *J. Fluid Mech.* **1988**, *195*, 223–237. [[CrossRef](#)] [[PubMed](#)]
34. Kessler, J.O. Hydrodynamic focusing of motile algal cells. *Nature* **1985**, *313*, 218–220. [[CrossRef](#)]
35. Kessler, J.O. Co-operative and concentrative phenomena of swimming micro-organisms. *Contemp. Phys.* **1985**, *10*, 202–210. [[CrossRef](#)]
36. Hill, N.A.; Pedley, T.J.; Kessler, J.O. Growth of bioconvection patterns in a suspension of gyrotactic microorganisms in a layer of finite depth. *J. Fluid Mech.* **1989**, *208*, 509–543. [[CrossRef](#)]

37. Ghorai, S.; Hill, N.A. Development and stability of gyrotactic plumes in bioconvection. *J. Fluid Mech.* **1999**, *400*, 1–31. [[CrossRef](#)]
38. Ghorai, S.; Hill, N.A. Wavelengths of gyrotactic plumes in bioconvection. *Bull. Math. Biol.* **2000**, *62*, 429–450. [[CrossRef](#)]
39. Ghorai, S.; Hill, N.A. Gyrotactic bioconvection in three dimensions. *Phys. Fluid* **2007**, *19*, 054107. [[CrossRef](#)]
40. Hillesdon, A.; Pedley, T.J. Bioconvection in suspensions of oxytactic bacteria: Linear theory. *J. Fluid Mech.* **1996**, *324*, 223–259. [[CrossRef](#)]
41. Hopkins, M.M.; Fauci, L.J. A computational model of the collective fluid dynamics of motile micro-organisms. *J. Fluid Mech.* **2002**, *455*, 149–174. [[CrossRef](#)]
42. Kuznetsov, A.V. The onset of bioconvection in a suspension of gyrotactic microorganisms in a fluid layer of finite depth heated from below. *Int. Commun. Heat Mass Transf.* **2005**, *32*, 574–582. [[CrossRef](#)]
43. Zeng, L.; Pedley, T.J. Distribution of gyrotactic micro-organisms in complex three-dimensional flows. Part 1. Horizontal shear flow past a vertical circular cylinder. *J. Fluid Mech.* **2018**, *852*, 358–397. [[CrossRef](#)]
44. Sheremet, M.; Grosan, T.; Pop, I. MHD free convection flow in an inclined square cavity filled with both nanofluids and gyrotactic microorganisms. *Int. J. Numer. Method Heat* **2019**. submitted for publication. [[CrossRef](#)]
45. Sheremet, M.A.; Pop, I. Thermo-bioconvection in a square porous cavity filled by oxytactic microorganisms. *Transp. Porous Med.* **2014**, *103*, 191–205. [[CrossRef](#)]
46. Kuznetsov, A.V. The onset of nanofluid bioconvection in a suspension containing both nanoparticles and gyrotactic microorganisms. *Int. Commun. Heat Mass Transf.* **2010**, *37*, 1421–1425. [[CrossRef](#)]
47. Zaimi, K.; Ishak, A.; Pop, I. Stagnation-point flow toward a stretching/shrinking sheet in a nanofluid containing both nanoparticles and gyrotactic microorganisms. *J. Heat Transf.* **2014**, *136*, 041705. [[CrossRef](#)]
48. Ali, F.; Zaib, A. Unsteady flow of an Eyring-Powell nanofluid near stagnation point past a convectively heated stretching sheet. *Arab. J. Basic Appl. Sci.* **2019**, *26*, 215–224. [[CrossRef](#)]
49. Singh, M.K.; Natesan, S. Richardson extrapolation technique for singularly perturbed system of parabolic partial differential equations with exponential boundary layers. *Appl. Math. Comput.* **2018**, *333*, 254–275. [[CrossRef](#)]
50. Ibrahim, W.; Shankar, B.; Nandeppanavar, M.M. MHD stagnation point flow and heat transfer due to nanofluid towards a stretching sheet. *Int. J. Heat Mass Transf.* **2013**, *56*, 1–9. [[CrossRef](#)]



© 2019 by the authors. Licensee MDPI, Basel, Switzerland. This article is an open access article distributed under the terms and conditions of the Creative Commons Attribution (CC BY) license (<http://creativecommons.org/licenses/by/4.0/>).